Polarization constraints on the X-ray corona in Seyfert Galaxies: MCG-05-23-16

A. Marinucci,[1]★ F. Muleri,[2] M. Dovčiak,[3] S. Bianchi,[4] F. Marin,[5] G. Matt,[4] F. Ursini,[4]
R. Middei,[6,7] H. L. Marshall,[8] L. Baldini,[9,10] T. Barnouin,[5] N. Cavero Rodriguez,[11]
A. De Rosa,[2] L. Di Gesu,[1] D. Harper,[11] A. Ingram,[12] V. Karas,[3] H. Krawczynski,[11]
G. Madejski,[13] C. Panagiotou,[8] P. O. Petrucci,[14] J. Podgorny,[5,3,15] S. Puccetti,[6]
F. Tombesi,[16,17,18] A. Veledina,[19,20,21] W. Zhang,[22] I. Agudo,[23] L. A. Antonelli,[7,6]
M. Bachetti,[24] W. H. Baumgartner,[25] R. Bellazzini,[9] S. D. Bongiorno,[25] R. Bonino,[26,27]
A. Brez,[9] N. Bucciantini,[28,29,30] F. Capitanio,[2] S. Castellano,[9] E. Cavazzuti,[1]
S. Ciprini,[17,6] E. Costa,[2] E. Del Monte,[2] N. Di Lalla,[13] A. Di Marco,[2] I. Donnarumma,[1]
V. Doroshenko,[31,21] S. R. Ehlert,[25] T. Enoto,[32] Y. Evangelista,[2] S. Fabiani,[2]
R. Ferrazzoli,[2] J. A. Garcia,[33] S. Gunji,[34] K. Hayashida,[35] J. Heyl,[36] W. Iwakiri,[37]
S. G. Jorstad,[38,39] T. Kitaguchi,[32] J. J. Kolodziejczak,[25] F. La Monaca,[2] L. Latronico,[26]
I. Liodakis,[40] S. Maldera,[26] A. Manfreda,[9] A. P. Marscher,[38] I. Mitsuishi,[41] T. Mizuno,[42]
C.-Y. Ng,[43] S. L. O'Dell,[25] N. Omodei,[13] C. Oppedisano,[26] A. Papitto,[7] G. G. Pavlov,[44]
A. L. Peirson,[13] M. Perri,[6,7] M. Pesce-Rollins,[9] M. Pilia,[24] A. Possenti,[24]
J. Poutanen,[19,21] B. D. Ramsey,[25] J. Rankin,[2] A. Ratheesh,[2] R. W. Romani,[13] C. Sgrò,[9]
P. Slane,[45] P. Soffitta,[2] G. Spandre,[9] T. Tamagawa,[32] F. Tavecchio,[46] R. Taverna,[47]
Y. Tawara,[41] A. F. Tennant,[25] N. E. Thomas,[25] A. Trois,[24] S. S. Tsygankov,[19,21]
R. Turolla,[47,48] J. Vink,[49] M. C. Weisskopf,[25] K. Wu,[48] F. Xie,[50,2] S. Zane[48]

ABSTRACT

We report on the first observation of a radio-quiet Active Galactic Nucleus (AGN) using polarized X-rays: the Seyfert 1.9 galaxy MCG-05-23-16. This source was pointed with the *Imaging X-ray Polarimetry Explorer* (*IXPE*) starting on May 14, 2022 for a net observing time of 486 ks, simultaneously with XMM-*Newton* (58 ks) and *NuSTAR* (83 ks). A polarization degree smaller than $\Pi < 4.7\%$ (at the 99% c.l.) is derived in the 2-8 keV energy range, where emission is dominated by the primary component ascribed to the hot corona. The broad-band spectrum, inferred from a simultaneous fit to the *IXPE*, *NuSTAR*, and XMM-*Newton* data, is well reproduced by a power law with photon index $\Gamma = 1.85 \pm 0.01$ and a high-energy cutoff $E_C = 120 \pm 15$ keV. A comparison with Monte Carlo simulations shows that a lamp-post and a conical geometry of the corona are consistent with the observed upper limit, a slab geometry is allowed only if the inclination angle of the system is less than 50°.

Key words: Galaxies: active - Galaxies: Seyfert - Individual: MCG-05-23-16

1 INTRODUCTION

It is now widely accepted that the primary X-ray emission of Seyfert galaxies is produced by multiple up-scattering events of cool pho-

★ E-mail: andrea.marinucci@asi.it (AM)

tons by hot electrons: the Comptonization process (Sunyaev & Titarchuk 1980; Zdziarski et al. 2000). However, the energy supply of this medium and the conditions leading to a formation of the hot plasma close to the black hole are debated. The physical picture of plasma fuelling through the gravitational energy transformation greatly depends on the geometry and size of the hot medium. In one scenario, the energy dissipation (and electron heating) is distributed over a large volume, with characteristic sizes $\sim 10-100\, R_g$ (where $R_g = GM/c^2$ is the gravitational radius, G is the gravitational constant, M is black hole mass and c is the speed of light). Early studies considered the so-called *slab-corona* model, where the hot medium was assumed to be distributed above the cold accretion disc (Haardt & Maraschi 1991, 1993), and presumably energized by some disc instability, likely of magnetic origin (Merloni 2003). On the other hand, in a *lamp-post* geometry, the primary X-ray emission is assumed to be coming from a compact source ($\sim 1-10\, R_g$), located on the accretion disc axis (Fabian et al. 2017b) and could be associated with an aborted jet (Ghisellini et al. 2004).

Spectroscopic analyses have in principle the capability to constrain the coronal geometry but, even the best available observations provided by *NuSTAR*, while good enough to measure the physical coronal parameters like the optical depth and the temperature, are not able to distinguish statistically among different geometries (Tortosa et al. 2018; Middei et al. 2019).

A very promising and powerful tool to assess the coronal geometry is reverberation mapping of the corona-disc system (Uttley et al. 2014, and references therein). In fact, the disc response to the corona illumination depends also on the geometry of the latter (Wilkins et al. 2016). However, to fully exploit this technique, observations with the next generation X-ray observatories such as *eXTP* and *Athena* are required (De Rosa et al. 2019; Dovciak et al. 2013), even if very long XMM-*Newton* observations can already deliver some results (Fabian et al. 2017a).

X-ray polarization provides an independent tool to constrain the coronal geometry. Polarization, in fact, is extremely sensitive to the geometry of the emitting matter and of the photon field (Schnittman & Krolik 2010; Beheshtipour et al. 2017; Tamborra et al. 2018; Zhang et al. 2019). With the aim to constrain its coronal geometry, the *Imaging X-ray Polarimetry Explorer* (*IXPE*: Weisskopf et al. 2016) observed the bright Seyfert galaxy MCG-05-23-16.

MCG-05-23-16 is a nearby (z=0.0085 or 36 Mpc, Wegner et al. 2003) Seyfert 1.9 galaxy with broad emission lines in the near-infrared (Goodrich et al. 1994). It has been extensively observed in X-rays (Weaver et al. 1997; Balestra et al. 2004; Braito et al. 2007; Reeves et al. 2007; Perola et al. 2002; Beckmann et al. 2008; Molina et al. 2013), showing a moderate cold absorption ($N_H \sim 10^{22}$ cm^{-2}). Recently, *NuSTAR* observations were able to constrain the high energy cutoff ($E_C \sim 100-160$ keV, variable on a time scale of $\sim$100 ks) and therefore the coronal physical parameters kT$_e$ and τ (Baloković et al. 2015; Zoghbi et al. 2017). X-ray reverberation features have also been detected with XMM-*Newton* in this source (Zoghbi et al. 2013; Kara et al. 2016).

In the optical and near-infrared wavelengths ($0.4-2.2\mu$m) the source exhibits a low continuum linear polarization degree ($1-2$%) and a polarized flux density which increases with wavelength, a possible sign of Compton scattering or a different non-thermal component at work (Brindle et al. 1990).

With a $2-10$ keV flux of $(7-10)\times10^{-11}$ erg cm^{-2} s^{-1} (Mattson & Weaver 2004), MCG-05-23-16 is one of the brightest Seyfert galaxies, only moderately variable on both short and long timescales, with a relatively simple spectrum (no significant absorption

in the *IXPE* band) and well measured coronal parameters. It is therefore the ideal target to search for polarization signatures of the coronal geometry in radio-quiet AGN. The paper is organized as follows: in Sect. 2 we discuss the data reduction procedure, while in Sect. 3 we present the spectro-polarimetric analyses. Our results are then discussed and summarized in Sect. 4 and 5.

2   OBSERVATIONS AND DATA REDUCTION

IXPE (Weisskopf et al. 2022) observed MCG-05-23-16 starting on May 14, 2022 with its three Detector Units (DU), for a net exposure time of 47 ks. The pointing of the source started again on May 21, for additional 439 ks. Cleaned level 2 event files were produced and calibrated using standard filtering criteria with the dedicated FTOOLS tasks and the latest calibration files available in the *IXPE* calibration database (CALDB 20211118). I, Q, U Stokes background spectra were extracted from source-free circular regions with a radius of 100 arcsec. Extraction radii for the I Stokes spectra of the source were computed via an iterative process which leads to the maximization of the Signal-to-Noise Ratio (SNR) in the 2-8 keV energy band, similar to the approach described in Piconcelli et al. (2004). We therefore adopted circular regions centered on the source with radii of 62 arcsec, 57 arcsec and 62 arcsec for DU1, DU2 and DU3, respectively. The net exposure times are 485.7 ks and the same extraction radii were then applied to the Q and U Stokes spectra. We used a constant energy binning of 0.2 keV for Q, U Stokes spectra and required a SNR higher than 5 in each spectral channel, in the intensity spectra. I, Q, U Stokes spectra from the three DUs are always fitted independently in the following, but we will plot them together using the SETP GROUP command in XSPEC, for the sake of visual clarity. Background represents the 2.0%, 1.8% and 2.1% of the total DU1, DU2 and DU3 I spectra, respectively. The summed background subtracted light curves show an average count rate $C_{2-8\, keV}$=0.525±0.002 cts s^{-1} with a level of variability of $\sim$20–30%, in the range 0.33-0.79 cts s^{-1}.

XMM-*Newton* started its observation on May 21, 2022 for 83 ks of elapsed time with the EPIC CCD cameras: the pn (Strüder et al. 2001) and the two MOS (Turner et al. 2001), operated in small window and medium filter mode. Data from the MOS detectors are not included in our analysis due to pile-up. The data from the pn camera show no significant pile-up as indicated by the EPATPLOT output. The extraction radii and the optimal time cuts for flaring particle background were computed with SAS 20 (Gabriel et al. 2004) with the same SNR maximization procedure reported above. The resulting optimal extraction radii for the source and the background spectra are 40 and 50 arcsec, respectively. The net exposure time for the pn time-averaged spectrum is 58.1 ks.

NuSTAR (Harrison et al. 2013) observed MCG-05-23-16 simultaneously to XMM-*Newton*, with its two coaligned X-ray telescopes with corresponding Focal Plane Module A (FPMA) and B (FPMB). The total elapsed time is 171.4 ks. The Level 1 data products were processed with the *NuSTAR* Data Analysis Software (NuSTARDAS) package (v. 2.1.2). Cleaned event files (level 2 data products) were produced and calibrated using standard filtering criteria with the NUPIPELINE task and the latest calibration files available in the *NuSTAR* calibration database (CALDB 20220510). Extraction radii for the source and background spectra were 40 arcsec and 60 arcsec, FPMA spectra were binned in order not to over-sample the instrumental resolution more than a factor of 2.5 and to have a SNR greater than 5 in each spectral channel, the same energy binning was then applied to the FPMB spectra. The net observing times for the
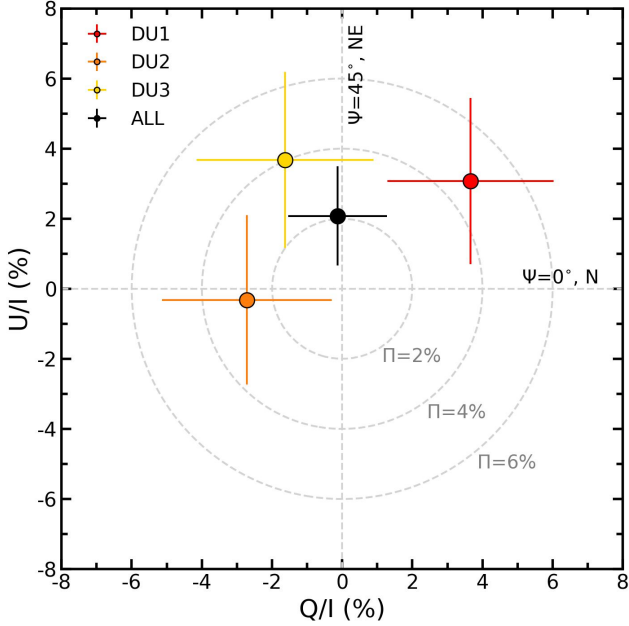
Figure 1. Normalized U/I and Q/I Stokes parameters are shown, calculated using the full 2-8 keV *IXPE* band. Uncertainties are reported at the 68% c.l.

FPMA and the FPMB data sets are 83.4 ks and 83 ks, respectively. We adopt the cosmological parameters $H_0 = 70$ km s^{-1} Mpc^{-1}, $\Omega_\Lambda = 0.73$ and $\Omega_m = 0.27$, i.e. the default ones in XSPEC 12.12.1 (Arnaud 1996). Errors correspond to the 90% confidence level for one interesting parameter ($\Delta\chi^2 = 2.7$), if not stated otherwise.

3 DATA ANALYSIS

3.1 *IXPE* polarimetric analysis

We start investigating the polarized signal from MCG-05-23-16 by analyzing its polarization cubes, which are the simplest data structures holding polarization information. They can be created using IXPEOBSSIM (version 26.3.3: Baldini et al. 2022). This applies the Kislat et al. (2015) formalism to a user-defined set of events to compute the Stokes parameters, the Minimum Detectable Polarization (MDP: Elsner et al. 2012), the polarization degree, the polarization angle, and the associated uncertainties. In our case, we created one polarization cube for each DU and then one combining the three, using the whole $2-8$ keV band. Fig. 1 shows the normalized U/I and Q/I Stokes parameters, data counts from background regions have been subtracted. Using the polarization cube from the three combined DUs, we retrieve a MDP=4.3%, a polarization degree $\Pi = (2.1 \pm 1.4)$% and angle $\Psi = (47 \pm 19)°$ (using 68% c.l. on one single parameter). We do not constrain any energy dependence of the polarization properties.

3.2 XMM-*Newton*, *NuSTAR* and *IXPE* spectro-polarimetric analysis

We started modelling the simultaneous $2-10$ keV XMM-*Newton* and $3-79$ keV *NuSTAR* spectra of MCG-05-23-16 with a model composed of an absorbed cutoff power law (zTBABS × CUTOFFPL in XSPEC) and a Compton reflection component (XILLVER: García et al. 2013). The former reproduces the primary continuum of the source

Parameter	Best fitting values	
	CUTOFF POWER LAW	
N_H (cm^{-2})	$(1.35 \pm 0.05) \times 10^{22}$	
Γ	1.85 ± 0.01	
E_C (keV)	120 ± 15	
N	$(2.60 \pm 0.05) \times 10^{-2}$	
Π (%)	2.2 ± 1.7	
Ψ (°)	50 ± 25	
	XILLVER	
R	0.30 ± 0.05	
N	$2.14^{+0.4}_{-0.1} \times 10^{-2}$	
Π (%)	-	
Ψ (°)	-	
	KERRDISK	
θ (°)	48^{+12}_{-8}	
N	$(3.9\pm^{+0.8}_{-0.5}) \times 10^{-5}$	
Π (%)	-	
Ψ (°)	-	
χ^2/dof	$1250/1169$	
F_{2-10} (erg cm^{-2} s^{-1})	$(7.45 \pm 0.05) \times 10^{-11}$	
L_{2-10} (erg s^{-1})	$(1.20 \pm 0.02) \times 10^{43}$	
	CROSS-CALIBRATIONS	
CONSTANTS		GAIN
C_{pn-DU1} $1.09^{+0.02}_{-0.01}$		α_{DU1} 0.953 ± 0.009
C_{pn-DU2} 1.06 ± 0.02		β_{DU1} 0.07 ± 0.03
C_{pn-DU3} 0.97 ± 0.02		α_{DU2} $0.963^{+0.007}_{-0.009}$
$C_{pn-FPMA}$ 1.39 ± 0.01		β_{DU2} 0.04 ± 0.03
$C_{pn-FPMB}$ 1.43 ± 0.01		α_{DU3} $0.951^{+0.009}_{-0.007}$
		β_{DU3} $0.07^{+0.03}_{-0.04}$

Table 1. Best fit parameters from the joint fit. Normalization units are in photons keV^{-1} cm^{-2} s^{-1}. R is the reflection fraction measured as the ratio between the Compton reflection and the primary component fluxes between 20 and 40 keV. The $2-10$ keV flux is retrieved from the EPIC-pn data.

while the latter takes into account reflection off neutral, distant material. Galactic absorption is modeled with TBABS, using a column density $N_H = 7.8 \times 10^{20}$ cm^{-2} (HI4PI Collaboration et al. 2016) and multiplicative constants take into account cross-calibration uncertainties between the FPMA, the FPMB and EPIC pn. The photon index and cutoff energy of the reflection continuum is linked to the one of the primary continuum, iron abundance is fixed to the solar one and the inclination angle to $\theta = 30°$. The resulting χ^2/dof is good (785/628) but some residuals appear at ~6 keV[1]. This could be indicative of a second iron Kα component, smeared by relativistic effects in the inner regions of the accretion disc. Indeed, when compared with old XMM data, residuals are perfectly consistent with the ones presented in Braito et al. (2007). A further spectral component is therefore included: (KERRDISK: BRENNEMAN & REYNOLDS 2006). The black hole spin is fixed to $a = 0.998$, the emissivity to $\epsilon(r) = r^{-3}$, the rest-frame energy of the emission line at 6.4 keV and the inner radius of the disc to $R_{in} = 37$ R_g (as reported in the simultaneous XMM+Suzaku analysis: Reeves et al. 2007). We obtain a best fit χ^2/dof=683/625 (Fig. 2) and an inclination angle $\theta = 48^{+12}_{-8}°$. A more detailed analysis of the complete data set will be presented in a forthcoming paper.

---

[1] The inferred energy of the Fe Kα line in the pn spectrum is not consistent with 6.4 keV and we therefore added a VASHIFT component in the model. We retrieve $v = 2230^{+510}_{-550}$ km s^{-1}. Since this effect is not found in the MOS spectra we conclude that is likely due to calibration issues in the pn.
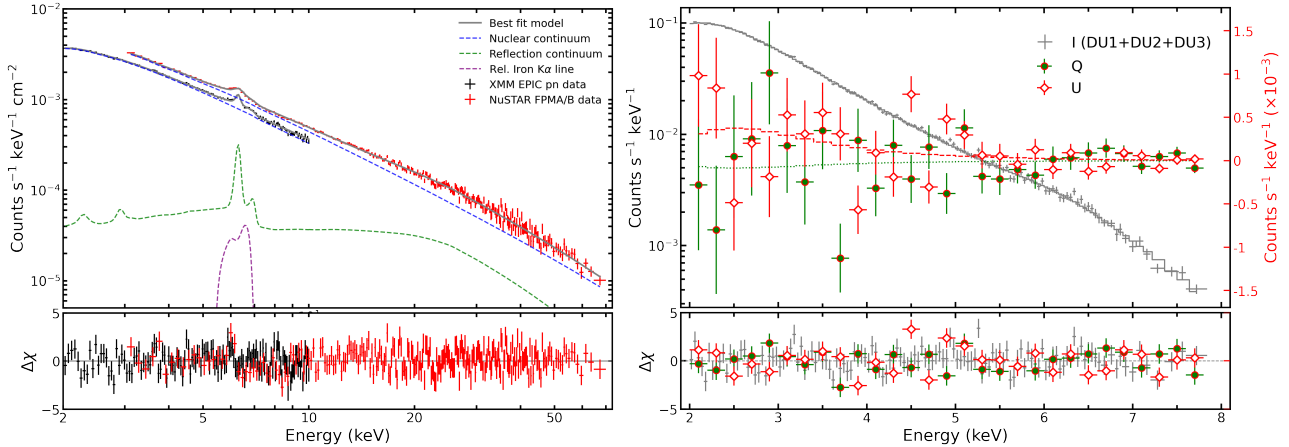
Figure 2. *Left panel:* The simultaneous EPIC pn and the grouped *NuSTAR* FPMA and FPMB spectra of MCG-05-23-16 divided by the relative effective area are shown with residuals. The best fitting model is shown as a solid grey line and the different components as dashed lines. *Right panel: IXPE I* (grey circles), *Q* (green circles) and *U* (red empty circles) grouped Stokes spectra are shown with residuals, along with the corresponding best fitting models. Note the different scales on the *y*-axes for *I* and *Q/U* data.

We then included *IXPE I* Stokes spectra to the XMM and *NuSTAR* fit. We followed the formalism discussed in Strohmayer (2017) and used the weighted analysis method presented in Di Marco et al. (2022) (parameter stokes=Neff in xselect). We obtain a χ^2/dof=1378/1000 due to presence of large residuals at the low and high energies in the *IXPE I* spectra. This has already been observed in other bright sources and can be likely explained in terms of calibration issues (Taverna et al. 2022; Krawczynski et al. 2022). We therefore modified the response files gains in the *I* spectra (using gain fit command) and obtained a χ^2/dof=1055/994. We then included the *Q* and *U* Stokes spectra and linked their gain parameters to the ones of the *I* spectra. Cross-calibration constants are included and the three spectral components of the model are convolved with the polarization model polconst. Two parameters can be then be inferred for each spectral component: the polarization degree Π and angle Ψ, both constant functions of the energy. The polarization degree and angle associated to the nuclear continuum are left free to vary while the ones associated to the other spectral components are fixed to Π = 0% and Ψ = 0°. We will verify a posteriori that the fit is insensitive to these values. We retrieve the photon index Γ = 1.85 ± 0.01 and the cutoff energy E_C = 120 ± 15 keV, in agreement with previously reported values (Baloković et al. 2015; Zoghbi et al. 2017). The best spectro-polarimetric joint fit provides the polarization degree Π=(2.2 ± 1.7)% and Ψ=(50 ± 25)° for the nuclear power law. Therefore, at the 99% c.l. (for one single parameter of interest, $\Delta\chi^2$ = 6.63) we only get an upper limit Π = 4.7%. The contour plots between these two parameters are shown in Fig. 3. If the cutoff power law is substituted by the Comptonization model compps (Poutanen & Svensson 1996) an electron temperature kT_e=25±2 keV and optical depth τ = 1.27 ± 0.08 are retrieved, assuming a slab geometry (χ^2/dof=1248/1169).

On theoretical grounds, the Compton reflection continuum is expected to be moderately polarized but the iron Kα fluorescence emission line arising from the same scattering material is not (as shown in Goosmann & Matt 2011; Marin 2018). We also note that scattering from distant AGN components do not significantly impact the measured polarization due to their low contribution in this energy band (Marin et al. 2018). However, we also tried to leave the polarization degree of the xillver and kerrdisk components free to vary in the fit. No statistically significant improvement is

found (χ^2/dof=1250/1169) and the fit is insensitive to these two parameters.

4 DISCUSSION

Several radio-loud AGN have been observed in the first *IXPE* months of operations and a highly significant polarized signal has been measured in two blazars so far, due to synchrotron emission in the jet. On the other hand, polarized X-rays produced in radio quiet sources are thought to be produced by the inverse Compton mechanism, occurring within tens of gravitational radii from the central black hole. Different geometries of the scattering medium, depending on the degree of asymmetry, will result in a different degree of polarization.

MCG-05-23-16 is the first radio quiet AGN observed by *IXPE* and the nuclear power law component, ascribed to the hot corona, contributes to the 94±3% of the 2-8 keV flux. We found that the best spectro-polarimetric fit of the simultaneous *IXPE-NuSTAR*-XMM data provides only, at the 99% c.l., an upper limit Π = 4.7%. Three different geometries for the hot corona in this AGN have been recently explored in Ursini et al. (2022), with the Comptonization code monk (Zhang et al. 2019). Fig. 3 shows the results with input coronal temperatures kT_e=25 keV and different Thomson optical depths τ, which correspond to the spectral shape of the continuum reported in Tab. 1. The three coronal geometries are: a slab sandwiching the accretion disc, a spherical lamp-post on the symmetry axis, and a truncated cone in outflow to describe the base of a failed jet. The geometrical parameters for the simulations shown in Fig. 3 are as follows. The slab corona fully covers a truncated disc with an inner radius of 30 R_g. The spherical lamp-post has a radius of 10 R_g and a height above the disc of 30 R_g. As for the truncated cone, the distance between the lower base and the disc and the vertical thickness are both of 20 R_g, while the semi-aperture is 30°, and the outflow velocity is 0.3c. Among these geometries, the slab corona is the only one that gives a polarization vector perpendicular to the disc plane, the other two predicting it to be parallel to the accretion disc. We note that the polarization angle for the three geometries does not significantly vary for different input kT_e and τ values, while the absolute value of the polarization degree can change. However, this
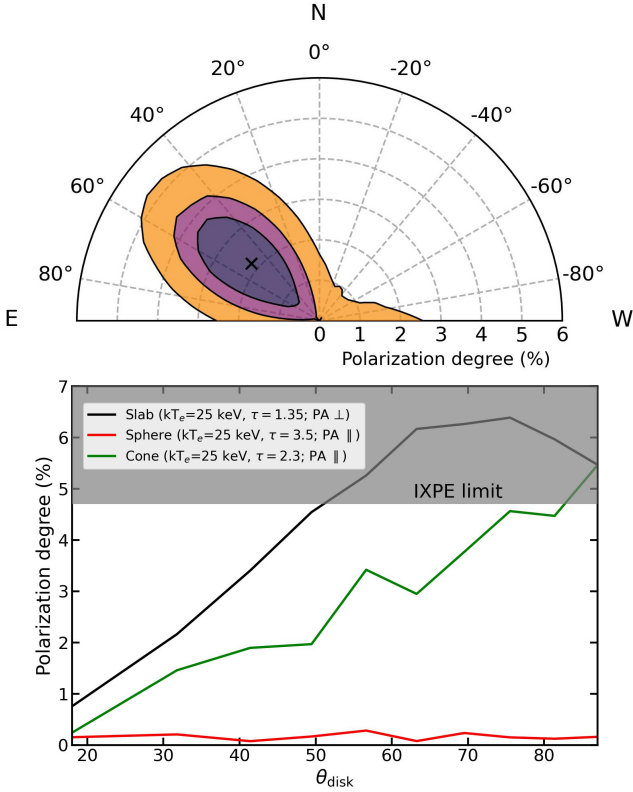
Figure 3. *Top-panel:* contour plot between the polarization degree Π and angle Ψ associated to the primary power law component. Purple, pink and orange shaded regions indicate 68%, 90% and 99% confidence levels for two parameters of interest, respectively. *Bottom-panel:* Monte Carlo simulations performed with the Comptonization code MONK. The input coronal parameters kT_e, τ correspond to the spectral shape reported in Tab. 1 and the polarization angle is reported with respect to the accretion disc plane.

does not impact much on the relative differences between the three geometries.

VLA observations at 8.4 GHz of the source showed a possible elongation in PA≃ 169° east of north (Mundell et al. 2009) while Hubble Space Telescope WFPC2 images revealed [O III] emission in PA≃ 40° (Ferruit et al. 2000). The 90% c.l. contour plot shows that the polarization angle is roughly aligned with the [O III] emitting region, which likely traces the Narrow Line Region (NLR) in this object. Assuming that the accretion disc is perpendicular to the NLR, a slab corona geometry would produce such a polarization angle, similar to what observed in the X-ray binary Cyg X-1 (Krawczynski et al. 2022). Of course, given the low significance of this result, it must be taken as no more than suggestive, needing more data for a confirmation. Highly inclined slab geometries (with $\theta \gtrsim 50°$) can be ruled out and our estimate of $\theta = 48^{+12}_{-8}°$, from the broad iron Kα profile, does not provide further constraints on the hot coronal geometry.

5 CONCLUSIONS

The launch of *IXPE*, on December 9, 2021, opened a new observing window on the study of supermassive black holes and MCG-05-23-16 is the perfect candidate to investigate the hot corona close to the supermassive black hole. Simultaneously observed with *IXPE*, XMM-*Newton* and *NuSTAR* in May 2022, the source showed a low level of neutral absorption along the line of sight ($N_H = 1.35\pm0.05\times 10^{22}$ cm^{-2}), a modest level of Compton reflection ($R = 0.30\pm0.05$)

and broad relativistic iron Kα emission line. This translates into a power-law continuum which largely dominates the total flux in the 2–8 keV *IXPE* band ($F_{pow}/F_{tot} = 94\pm3\%$) and when it is convolved with a constant polarization model we obtain a 99% c.l. upper limit to the polarization fraction of 4.7%. This result is consistent with a spherical ("lamp-post") and a conical geometry of the corona, while for a slab corona (with kT_e=25 keV and τ = 1.35) it implies an inclination angle less than 50°.

REFERENCES

Arnaud K. A., 1996, in ASP Conf. Ser. 101: Astronomical Data Analysis Software and Systems V. p. 17
Baldini L., Bucciantini N., Di Lalla N., Ehlert S. R., Manfreda A., Omodei N., Pesce-Rollins M., Sgrò C., 2022, arXiv e-prints, p. arXiv:2203.06384
Balestra I., Bianchi S., Matt G., 2004, A&A, 415, 437
Baloković M., et al., 2015, ApJ, 800, 62
Beckmann V., Courvoisier T. J. L., Gehrels N., Lubiński P., Malzac J., Petrucci P. O., Shrader C. R., Soldi S., 2008, A&A, 492, 93
Beheshtipour B., Krawczynski H., Malzac J., 2017, ApJ, 850, 14
Braito V., et al., 2007, ApJ, 670, 978
Brenneman L. W., Reynolds C. S., 2006, ApJ, 652, 1028
Brindle C., Hough J. H., Bailey J. A., Axon D. J., Ward M. J., Sparks W. B., McLean I. S., 1990, MNRAS, 244, 604
De Rosa A., et al., 2019, Science China Physics, Mechanics, and Astronomy, 62, 29504
Di Marco A., et al., 2022, AJ, 163, 170
Dovciak M., et al., 2013, arXiv e-prints, p. arXiv:1306.2331
Elsner R. F., O'Dell S. L., Weisskopf M. C., 2012, in Space Telescopes and Instrumentation 2012: Ultraviolet to Gamma Ray. p. 84434N (arXiv:1208.0610), doi:10.1117/12.924889
Fabian A. C., Alston W. N., Cackett E. M., Kara E., Uttley P., Wilkins D. R., 2017a, Astronomische Nachrichten, 338, 269
Fabian A. C., Lohfink A., Belmont R., Malzac J., Coppi P., 2017b, MNRAS, 467, 2566
Ferruit P., Wilson A. S., Mulchaey J., 2000, ApJS, 128, 139
Gabriel C., et al., 2004, in F. Ochsenbein, M. G. Allen, & D. Egret ed., Astronomical Society of the Pacific Conference Series Vol. 314, Astronomical Data Analysis Software and Systems (ADASS) XIII. pp 759–+
García J., Dauser T., Reynolds C. S., Kallman T. R., McClintock J. E., Wilms J., Eikmann W., 2013, ApJ, 768, 146
Ghiselini G., Haardt F., Matt G., 2004, A&A, 413, 535
Goodrich R. W., Veilleux S., Hill G. J., 1994, ApJ, 422, 521
Goosmann R. W., Matt G., 2011, MNRAS, 415, 3119

HI4PI Collaboration et al., 2016, A&A, 594, A116

Haardt F., Maraschi L., 1991, ApJ, 380, L51

Haardt F., Maraschi L., 1993, ApJ, 413, 507

Harrison F. A., et al., 2013, ApJ, 770, 103

Kara E., Alston W. N., Fabian A. C., Cackett E. M., Uttley P., Reynolds C. S., Zoghbi A., 2016, MNRAS, 462, 511

Kislat F., Clark B., Beilicke M., Krawczynski H., 2015, Astroparticle Physics, 68, 45

Krawczynski H., et al., 2022, arXiv e-prints, p. arXiv:2206.09972

Marin F., 2018, A&A, 615, A171

Marin F., Dovčiak M., Kammoun E. S., 2018, MNRAS, 478, 950

Mattson B. J., Weaver K. A., 2004, ApJ, 601, 771

Merloni A., 2003, MNRAS, 341, 1051

Middei R., Bianchi S., Marinucci A., Matt G., Petrucci P. O., Tamborra F., Tortosa A., 2019, A&A, 630, A131

Molina M., Bassani L., Malizia A., Stephen J. B., Bird A. J., Bazzano A., Ubertini P., 2013, MNRAS, 433, 1687

Mundell C. G., Ferruit P., Nagar N., Wilson A. S., 2009, ApJ, 703, 802

Perola G. C., Matt G., Cappi M., Fiore F., Guainazzi M., Maraschi L., Petrucci P. O., Piro L., 2002, A&A, 389, 802

Piconcelli E., Jimenez-Bailón E., Guainazzi M., Schartel N., Rodríguez-Pascual P. M., Santos-Lleó M., 2004, MNRAS, 351, 161

Poutanen J., Svensson R., 1996, ApJ, 470, 249

Reeves J. N., et al., 2007, PASJ, 59, 301

Schnittman J. D., Krolik J. H., 2010, ApJ, 712, 908

Strohmayer T. E., 2017, ApJ, 838, 72

Strüder L., et al., 2001, A&A, 365, L18

Sunyaev R. A., Titarchuk L. G., 1980, A&A, 86, 121

Tamborra F., Matt G., Bianchi S., Dovčiak M., 2018, A&A, 619, A105

Taverna R., et al., 2022, arXiv e-prints, p. arXiv:2205.08898

Tortosa A., Bianchi S., Marinucci A., Matt G., Petrucci P. O., 2018, A&A, 614, A37

Turner M. J. L., et al., 2001, A&A, 365, L27

Ursini F., Matt G., Bianchi S., Marinucci A., Dovčiak M., Zhang W., 2022, MNRAS, 510, 3674

Uttley P., Cackett E. M., Fabian A. C., Kara E., Wilkins D. R., 2014, A&ARv, 22, 72

Weaver K. A., Yaqoob T., Mushotzky R. F., Nousek J., Hayashi I., Koyama K., 1997, ApJ, 474, 675

Wegner G., et al., 2003, AJ, 126, 2268

Weisskopf M. C., et al., 2016, Results in Physics, 6, 1179

Weisskopf M. C., et al., 2022, Journal of Astronomical Telescopes, Instruments, and Systems, 8, 026002

Wilkins D. R., Cackett E. M., Fabian A. C., Reynolds C. S., 2016, MNRAS, 458, 200

Zdziarski A. A., Poutanen J., Johnson W. N., 2000, ApJ, 542, 703

Zhang W., Dovčiak M., Bursa M., 2019, ApJ, 875, 148

Zoghbi A., Reynolds C., Cackett E. M., Miniutti G., Kara E., Fabian A. C., 2013, ApJ, 767, 121

Zoghbi A., et al., 2017, ApJ, 836, 2

Affiliations:

[1] ASI - Agenzia Spaziale Italiana, Via del Politecnico snc, 00133 Roma, Italy

[2] INAF Istituto di Astrofisica e Planetologia Spaziali, Via del Fosso del Cavaliere 100, 00133 Roma, Italy

[3] Astronomical Institute of the Czech Academy of Sciences, Boční II 1401/1, 14100 Praha 4, Czech Republic

[4] Dipartimento di Matematica e Fisica, Università degli Studi Roma Tre, Via della Vasca Navale 84, 00146 Roma, Italy

[5] Université de Strasbourg, CNRS, Observatoire Astronomique de Strasbourg, UMR 7550, 67000 Strasbourg, France

[6] Space Science Data Center, Agenzia Spaziale Italiana, Via del Politecnico snc, 00133 Roma, Italy

[7] INAF Osservatorio Astronomico di Roma, Via Frascati 33, 00078 Monte Porzio Catone (RM), Italy

[8] MIT Kavli Institute for Astrophysics and Space Research, Massachusetts Institute of Technology, 77 Massachusetts Avenue, Cambridge, MA 02139, USA

[9] Istituto Nazionale di Fisica Nucleare, Sezione di Pisa, Largo B. Pontecorvo 3, 56127 Pisa, Italy

[10] Dipartimento di Fisica, Università di Pisa, Largo B. Pontecorvo 3, 56127 Pisa, Italy

[11] Physics Department and McDonnell Center for the Space Sciences, Washington University in St. Louis, St. Louis, MO 63130, USA

[12] School of Mathematics, Statistics, and Physics, Newcastle University, Newcastle upon Tyne NE1 7RU, UK

[13] Department of Physics and Kavli Institute for Particle Astrophysics and Cosmology, Stanford University, Stanford, California 94305, USA

[14] Université Grenoble Alpes, CNRS, IPAG, 38000 Grenoble, France

[15] Astronomical Institute, Charles University, V Holešovičkách 2, CZ-18000 Prague, Czech Republic

[16] Dipartimento di Fisica, Università degli Studi di Roma "Tor Vergata", Via della Ricerca Scientifica 1, 00133 Roma, Italy

[17] Istituto Nazionale di Fisica Nucleare, Sezione di Roma "Tor Vergata", Via della Ricerca Scientifica 1, 00133 Roma, Italy

[18] Department of Astronomy, University of Maryland, College Park, Maryland 20742, USA

[19] Department of Physics and Astronomy, 20014 University of Turku, Finland

[20] Nordita, KTH Royal Institute of Technology and Stockholm University, Hannes Alfvéns väg 12, SE-10691 Stockholm, Sweden

[21] Space Research Institute of the Russian Academy of Sciences, Profsoyuznaya Str. 84/32, Moscow 117997, Russia

[22] National Astronomical Observatories, Chinese Academy of Sciences, 20A Datun Road, Beijing 100101, China

[23] Instituto de Astrofísica de Andalucía—CSIC, Glorieta de la Astronomía s/n, 18008 Granada, Spain

[24] INAF Osservatorio Astronomico di Cagliari, Via della Scienza 5, 09047 Selargius (CA), Italy

[25] NASA Marshall Space Flight Center, Huntsville, AL 35812, USA

[26] Istituto Nazionale di Fisica Nucleare, Sezione di Torino, Via Pietro Giuria 1, 10125 Torino, Italy

[27] Dipartimento di Fisica, Università degli Studi di Torino, Via Pietro Giuria 1, 10125 Torino, Italy

[28] INAF Osservatorio Astrofisico di Arcetri, Largo Enrico Fermi 5, 50125 Firenze, Italy

[29] Dipartimento di Fisica e Astronomia, Università degli Studi di Firenze, Via Sansone 1, 50019 Sesto Fiorentino (FI), Italy

[30] Istituto Nazionale di Fisica Nucleare, Sezione di Firenze, Via Sansone 1, 50019 Sesto Fiorentino (FI), Italy

[31] Institut für Astronomie und Astrophysik, Universität Tübingen, Sand 1, 72076 Tübingen, Germany

[32] RIKEN Cluster for Pioneering Research, 2-1 Hirosawa, Wako, Saitama 351-0198, Japan

[33] California Institute of Technology, Pasadena, CA 91125, USA

[34] Yamagata University,1-4-12 Kojirakawa-machi, Yamagata-shi 990-8560, Japan

[35] Osaka University, 1-1 Yamadaoka, Suita, Osaka 565-0871, Japan

[36] University of British Columbia, Vancouver, BC V6T 1Z4, Canada

[37] Department of Physics, Faculty of Science and Engineering, Chuo University, 1-13-27 Kasuga, Bunkyo-ku, Tokyo 112-8551, Japan

[38] Institute for Astrophysical Research, Boston University, 725 Commonwealth Avenue, Boston, MA 02215, USA

[39] Department of Astrophysics, St. Petersburg State University, Universitetsky pr. 28, Petrodvoretz, 198504 St. Petersburg, Russia

[40] Finnish Centre for Astronomy with ESO, 20014 University of Turku, Finland

[41] Graduate School of Science, Division of Particle and Astrophysical Science, Nagoya University, Furo-cho, Chikusa-ku, Nagoya, Aichi 464-8602, Japan

[42] Hiroshima Astrophysical Science Center, Hiroshima University, 1-3-1 Kagamiyama, Higashi-Hiroshima, Hiroshima 739-8526, Japan

[43] Department of Physics, The University of Hong Kong, Pokfulam, Hong Kong

[44] Department of Astronomy and Astrophysics, Pennsylvania State University, University Park, PA 16802, USA

[45] Center for Astrophysics | Harvard & Smithsonian, 60 Garden St, Cambridge, MA 02138, USA

[46] INAF Osservatorio Astronomico di Brera, Via E. Bianchi 46, 23807 Merate (LC), Italy

[47] Dipartimento di Fisica e Astronomia, Università degli Studi di Padova, Via Marzolo 8, 35131 Padova, Italy

[48] Mullard Space Science Laboratory, University College London, Holmbury St Mary, Dorking, Surrey RH5 6NT, UK

[49] Anton Pannekoek Institute for Astronomy & GRAPPA, University of Amsterdam, Science Park 904, 1098 XH Amsterdam, The Netherlands

[50] Guangxi Key Laboratory for Relativistic Astrophysics, School of Physical Science and Technology, Guangxi University, Nanning 530004, China